

## A SELF-ADAPTIVE APPROACH FOR NUMERICAL DEVICE SIMULATION

K. Deljouie-Rakhshandeh

STC Technology Ltd., London Road, HARLOW,  
 ESSEX CM21 9NB, UK.

### SUMMARY

Various approaches to the computation of an error indicator for semiconductor device simulation are reviewed, and an error indicator closely related to the box method is presented. Practical aspects of a self-adaptive scheme such as mesh generation and interpolation are briefly discussed. And an adaptive scheme which uses the above concepts is demonstrated for a p-n diode, a MESFET and a MOSFET.

### LIST OF SYMBOLS

$\psi$	Electrostatic potential
$n, p$	Electron and hole density
$\mu_n, \mu_p$	Electron and hole mobilities
$\epsilon$	Total permittivity, $\epsilon = \epsilon_0 \epsilon_r$
$R$	Recombination-Generation rate
$N_D, N_A$	donor and acceptor densities
$D$	Doping density $D = (N_A - N_D) / n_i$ , where $n_i$ is the intrinsic density
$\Omega$	Domain of a device
$\partial\Omega$	Boundary of $\Omega$
$    \cdot    _{\Omega}$	Energy norm
$(u, v)_{\Omega}$	Inner product, $(u, v)_{\Omega} = \int_{\Omega} u \cdot v \, d\Omega$
$   \cdot   _{\Omega}$	$L_2$ norm, $  u  _{\Omega}^2 = (u, u)_{\Omega}$

All the parameters which appear in this paper;  $\psi$ ,  $n$ ,  $p$ ,  $D$ ,  $J_n$ ,  $J_p$  and  $E$  are normalized according to the DeMari's scaling, with the exception that all the space dimensions are scaled with respect to  $\lambda_{in} / \sqrt{\epsilon_r}$ , where  $\lambda_{in}$  is the intrinsic Debye length.

## 1. INTRODUCTION

The importance of adaptive refinement in the context of semiconductor device simulation is self-evident. It frees the user of the device simulation programme from the confines of designing and refining a mesh according to the device physics. In adaptive refinement, however, it is the solution of the device equations which dictates where the mesh should be fine and where it can be coarse. This decision is based on the computation of the error indicators. An error indicator is a measure of the solution error restricted to an individual element. All error indicators are computed using the available solution and prior to each stage of the grid refinement. The error indicators are, thus, *a-posteriori*. After each solution stage all error indicators are computed and those elements with the largest error are refined according to Fig. (1).

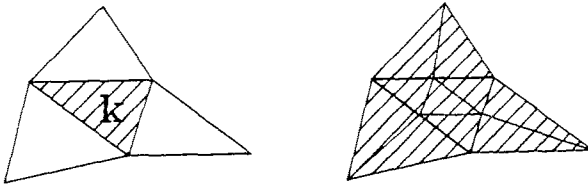


Figure 1- Refinement of element 'k'

This type of refinement is known as the h-version of finite element where a coarse grid gives rise to a more refined one, while the polynomial interpolants, on the elements of both grids, remain of the same degree.

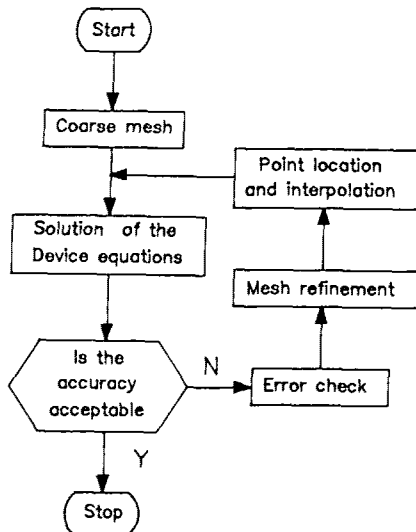


Figure 2- A Self-Adaptive Cycle

Grid refinement is proceeded by the interpolation of the available solution onto the new grid, which serves as an initial guess for the next solution-refinement stage. This cycle of solution-error check-refinement is shown in Fig. (2). Our emphasis in this paper is on the latter stages of this cycle, namely, the error indication, meshing, and the interpolation aspects of the refinement.

Published works on adaptive simulation of the semiconductor devices are rare and sparse. Those that we are aware of, are either based on computing the error solely for the Poisson equation (Guerrieri et al 1983), or are heuristic (Armstrong et al 1986), or are difficult to compute (Markowich 1986). Although recent advances in obtaining practical error indicators have influenced the related field of computational magneto-statics (Fernandes et al 1988), but the implication of such methods in device simulation is not clear. This problem is mainly caused by the fact that the semiconductor device equations form a coupled system and the continuity equation is not discretized by a standard finite element (FE) approach. In this paper we attempt to address this problem, where in the next section we present two approaches for error computation in semiconductor device simulation. The first, which is discussed in some detail in Deljouie-Rakhshandeh and Deeley (1988), is briefly reviewed here. The second approach which has the flavour of a box method, is simple to compute and easy to understand. In section 3 we also discuss the meshing and interpolation schemes used in this exercise. Our grid generation/refinement approach is aimed at creating an equi-angular triangulation, whereby the nodes belonging to the different stages of refinement do not coincide. We, therefore, discuss an interpolation algorithm which is used in the course of interpolating the results from one grid layout to another. In the last section, we provide computational examples using a p-n diode, a MOSFET, and a MESFET to examine our adaptive approach.

## 2. ERROR INDICATION

The setting for this work is the semiconductor device equations, which after appropriate normalization read:

$$(1a) \quad -\nabla \cdot (\epsilon_r \nabla \psi) = p-n-D \quad \text{in } \Omega,$$

$$(2) \quad \nabla \cdot (-\mu_n n \nabla \psi + \nabla n) = R \quad \text{in } \Omega,$$

$$(3) \quad \nabla \cdot (\mu_p p \nabla \psi + \nabla p) = R \quad \text{in } \Omega.$$

Eqn.(1) is the Poisson equation and (2) and (3) are the continuity equations for electrons and holes. The expressions enclosed in brackets in Eqn(2) and (3) are the corresponding current densities:

$$J_n = -\mu_n n \nabla \psi + \nabla n,$$

$$J_p = -\mu_p p \nabla \psi - \nabla p.$$

The Poisson equation is discretized by standard FE method where  $\Omega$  is partitioned into a set of triangles and a piecewise linear trial space  $S_h$  is employed for polynomial interpolation. Let the Poisson equation, (1a), support the following boundary conditions:

$$\varepsilon_r \frac{\partial \psi}{\partial n} = g \quad \text{on } \partial\Omega_N,$$

$$\psi = \psi_D \quad \text{on } \partial\Omega_D,$$

where  $\partial\Omega = \partial\Omega_D \cup \partial\Omega_N$  is the boundary of  $\Omega$ . A first solution to Eqn.(1),  $\psi_h = \bar{\psi} \mathbf{V}_h$  ( $\bar{\psi}$  is the vector of the nodal values, and  $\psi_h, \mathbf{V}_h \in S_h$ ), is obtained for a coarse grid.  $\psi_h$  satisfies the discrete weak form of Eqn.(1):

$$(4) \quad \sum_k (\varepsilon_r \nabla \psi_h, \nabla \mathbf{V}_h)_{\Omega_k} = \sum_k ((p-n+D), \mathbf{V}_h)_{\Omega_k} + \sum_k \int_{\partial\Omega_k \in \partial\Omega_N} g \cdot \mathbf{V}_h d\partial\Omega,$$

where  $\Omega_k$  is the area of element 'k' and  $\partial\Omega_k$  its boundary. The vector  $\mathbf{V}_h$  is the basis or shape function in the context of Galerkin method.

To compute an error indicator another piecewise polynomial space,  $S_q$ , on the triangulation is introduced, where  $S_q$  contains piecewise quadratic polynomials. The error in the electrostatic potential is then approximated as:

$$e_\psi = \psi_q - \psi_h; \text{ where } \psi_q \in S_q \text{ and } \psi_h \in S_h.$$

and the error is commonly measured in energy norm:

$$|||e_\psi|||_\Omega^2 = (\varepsilon_r \nabla e_\psi, \nabla e_\psi)_\Omega.$$

The error indicator is the restriction of the above norm to an element 'k':

$$\eta_{\psi,k}^2 = |||e_\psi|||_{\Omega_k}^2.$$

By employing the concept of hierarchical FE (Zienkiewicz and Craig 1986), an error indicator suitable for the Poisson equation and applicable to triangular grids has been suggested (Deljouie-Rakhshandeh and Deeley 1988):

$$(5) \quad \eta_{\psi,k}^2 = (3h_k^2 / 5\epsilon_r) \int_{\Omega_k} (n-p-D)^2 d\Omega + \\ (\sqrt{3} h_k / 12\epsilon_r) \int_{\partial\Omega_k} [\epsilon_r \partial\psi_h / \partial n]_j^2 d\partial\Omega,$$

where  $h_k$  is the element diameter and  $[\epsilon_r \partial\psi_h / \partial n]_j$  is the jump discontinuity in the component of the electric field normal to the element side. Eqn.(5) is not easily applicable to the continuity equations, but we have observed that the energy norm in  $e_\psi$  is related to the  $L_2$  norm of the error in the electric field:

$$|||e_\psi|||_{\Omega_k}^2 = \epsilon_r ||e_E||_{\Omega_k}^2,$$

and this was the setting for computing,  $||e_J||_{\Omega_k}$ , the  $L_2$  norm of the error in the current densities. In the Shrafetter-Gummel FE discretization of the continuity equations, the current density and the electric field on each element is assumed constant (Zlamal 1986). Despite this assumption, the final formulation leads to current densities whose nodal values differ on each element. The finite elements in this approach are more suited to the nodal assembly and a box interpretation of this leads to the much used method of control areas. In Deljouie-Rakhshandeh and Deeley (1988),  $||e_J||_{\Omega_k}$  was computed by first approximating a constant element current density:

$$(6) \quad J_0^K = \left( \sum_{r=1}^3 j_r A_r \right) / \Omega_k \quad \text{for} \quad \Omega_k = \sum_{r=1}^3 A_r,$$

where  $j_r$  are the nodal values of the current densities, and  $A_r$  are the area segments according to Fig.(3). Using the well known expression of Sharfetter and Gummel an edge current flowing from node 1 to node 2 was defined:

$$J_{E,3} = \mu_n [n_2 B(\delta_{21}) - n_1 B(\delta_{12})] / l_3,$$

where  $\delta_{21} = \bar{\psi}_2 - \bar{\psi}_1$  and  $B(\delta) = [\delta / (\exp(\delta) - 1)]$ . Using a linear vector basis function, the edge currents were interpolated within each element (Van Welij 1986):

$$(7) \quad J^k(x,y) = \sum_{i=1}^3 J_{E,r}^1 [ (y_r - y) \hat{i} + (x - x_r) \hat{j} ] / 2\Omega_k.$$

The error in the current density was therefore approximated by:

$$(8) \quad e_J = J^k(x,y) - J_0^k, \text{ and } \eta_{J,k}^2 = ||e_J||_{\Omega_k}^2.$$

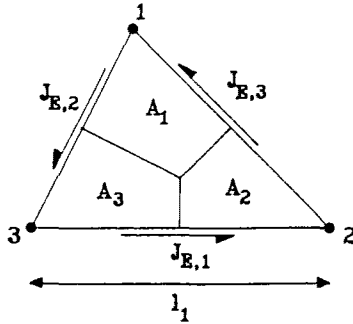


Figure 3- An element with its geometric and electric attributes

We now seek an alternative approach to treat the error in all the three semiconductor device equations consistently. First, consider the standard discretization of the Poisson equation with  $S_h$  as the trail space. Eqn.(4) leads to piecewise discontinuous constant electric field:

$$E_0 = \sum_k E_0^k \quad ; \quad k=1,2,\dots \text{ No. of elements,}$$

where  $E_0^k$  is constant inside element 'k' and zero outside. To obtain a better approximation to the electric field the projection method can be employed (Zienkiewicz and Zhu 1987), where the electric field is expanded by the same basis functions as the electrostatic potential:

$$E_h = V_h^t \bar{E},$$

where  $V_h = (V_h^1, V_h^2, \dots, V_h^n)^t$  and  $\bar{E} = (\bar{E}_1, \bar{E}_2, \dots, \bar{E}_n)^t$ , n is the total number of the elements, and  $E_h$  satisfies:

$$(9) \quad \int_{\Omega} V_h^t (E_h - E_0) d\Omega = 0.$$

The nodal values of the electric field,  $\bar{E}_i$ , can be computed by solving the n by n linear system resulting from Eqn.(9). Alternatively, evaluating all the integrals in (9) by nodal quadrature leads to the simple concept of nodal averaging which

is explained below: Consider a patch of elements,  $\text{supp}(i)$ , who share a node 'i' as shown in Fig.(4). The shaded region which is defined by the area allocations of Fig.(3) is call a 'box' whose area is  $b_i$ .

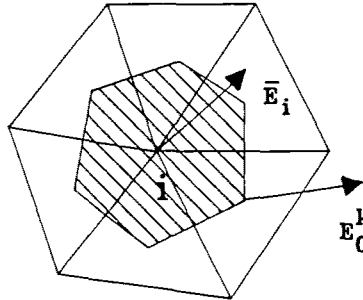


Figure 4- An Element Patch for the Node 'i'

The nodal averaging for this configuration reads:

$$(10) \quad \bar{E}_i = \left( \sum_{k \in \text{supp}(i)} E_0^k A_i^k \right) / b_i ; \quad b_i = \sum_{k \in \text{supp}(i)} A_i^k ,$$

where  $A_i^k$  is the area contribution of element 'k' to the box 'i'. An error indicator can now be defined as:

$$(11) \quad \eta_{E,k}^2 = ||e_E||_{\Omega_k}^2 = ((E_h - E_0^k), (E_h - E_0^k))_{\Omega_k} ,$$

and estimating (11) again by nodal quadrature leads to:

$$(12) \quad \eta_{E,k}^2 = \sum_i [(\bar{E}_i - E_0^k) \cdot (\bar{E}_i - E_0^k)] A_i^k ,$$

where  $i$  belongs to the node set of element 'k'. The error indicator of Eqn.(8) can readily be used in the context of the box method, and a similar error indicator for the current densities can be presented:

$$(13) \quad \eta_{J,k}^2 = ||e_J||_{\Omega_k}^2 = \sum_i [(\bar{J}_i - J_0^k) \cdot (\bar{J}_i - J_0^k)] A_i^k ,$$

where  $\bar{J}_i$  is the approximated nodal current density calculated in similar fashion to  $\bar{E}_i$  , and  $J_0^k$  is the constant element current density calculated as in Eqn.(6).

A comparison between the two error indicators, Eqn.(8) and Eqn.(12), for the continuity equation is instructive. In Eqn.(8) we exploit one main feature of the Sharfetter-Gummel FE discretization of the continuity equation in 2-D; that is the inequality of the nodal values of the current densities on each element. Since this feature of the S-G method is caused by the presence of the diffusion term in the continuity equation, for diffusion-free currents Eqn.(8) yields zero error. This is demonstrated by a simple experiment conducted on an L-shaped resistor. Here, there is a singularity at the vertex of the convex angle where the current densities increase in magnitude (Fig.(5a)). Starting from the coarse mesh of Fig(5b) the error indicator of Eqn.(8) yields zero error on all the elements, and the mesh remains unrefined. Using Eqn.(12), however, a non-zero  $\eta_{J,k}$  is measured for all the elements and three refinement cycles create the mesh shown in Fig.(5c), which reflects the variation of the current densities in the vicinity of the singular point.

Experiments with an adaptive strategy based on Eqn.(5) and (8) are presented in Deljouie-Rakhshandeh and Deeley (1988). Here, we concentrate on the use of Eqn.(12) and (13) as the principle error indicators. For a semiconductor device an error indicator should contain three components; one arising from the error in the Poisson equation and the other two from the error in the continuity equations. Various schemes can be devised to merge all the error contributions from Eqn.(12) and (13) into a refinement strategy. We have found a simple summation of the normalized error indicators useful, since it is compact and can easily be implemented in our refinement strategy.

$$(14) \quad \eta_k = \eta_{E,k} C_E^{-1} + \eta_{J_n,k} C_{J_n}^{-1} + \eta_{J_p,k} C_{J_p}^{-1},$$

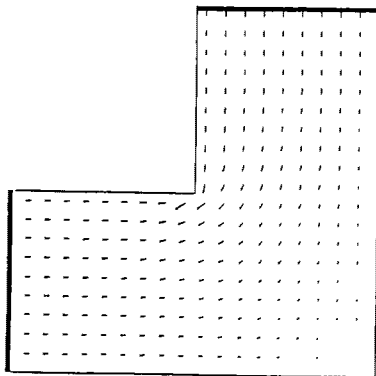
$$\text{where } C_E = 3 \text{ Max}(\eta_{E,1}, \eta_{E,2}, \dots, \eta_{E,n}),$$

$$C_{J_p} = 3 \text{ Max}(\eta_{J_p,1}, \eta_{J_p,2}, \dots, \eta_{J_p,n}),$$

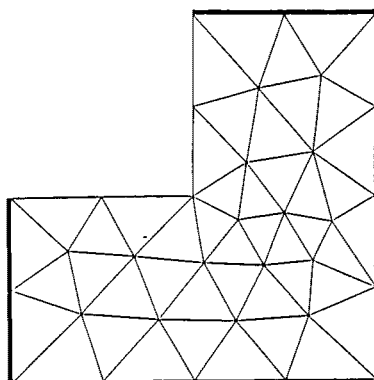
$C_{J_n}$  is similar to  $C_{J_p}$ , and 'n' in  $\eta_{E,n}$  is the total number of elements. The above constants normalize the error indicator, such the value of  $\eta_k$  on no element is greater than unity.

## 2. MESH GENERATION AND INTERPOLATION ASPECTS

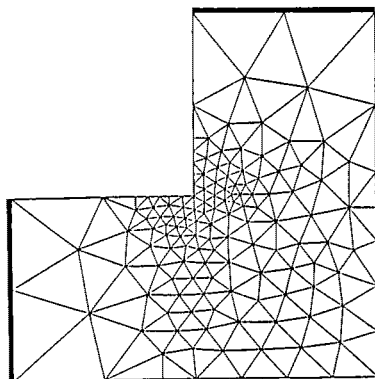
The mesh generator employed in this exercise aims at equi-angular triangulation and the resulting grid possesses very few obtuse triangles (Deljouie-Rakhshandeh 1988). This is achieved by extensive side-swapping and mesh-smoothing. In side-swapping the side subtending an obtuse angle is replaced by another bisecting it (Fig.(6)), and in mesh smoothing a node is moved



(a) Variation of the Current Densities.



(b) Initial Coarse Mesh.



(c) Refined Grid.

Figure 5- Grid Refinement for an L-Shped Resistor.

to the centre of gravity of the polygon created by its adjacent nodes (Fig.(7)).

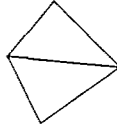
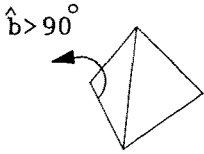


Figure 6- Side-Swapping

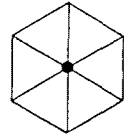
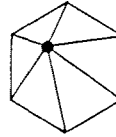


Figure 7- Mesh-Smoothing

Side-swapping and mesh-smoothing are performed at high speed by exploiting the adjacency information which the mesh generator creates. These are the Node-Node adjacency (NN) list which holds the list of those nodes adjacent to any one node, the Node-Element adjacency (NE) list which holds the list of those elements sharing a particular node, and the Element-Node adjacency (EN) list which holds the node number of the vertices of a particular element. Each refinement stage is proceeded by side-swapping and mesh-smoothing, which implies that the nodes on the newly refined grid, say  $G_{new}$ , do not coincide with the nodes of the previous grid,  $G_{old}$ . In order to create an initial guess for  $\psi$ ,  $n$ , and  $p$  on the new grid a point location and an interpolation process has to be performed. Our fast point location algorithm is constructed around the Element-Node adjacency list,  $EN(k,i)$ , where it returns the node number of the  $i^{th}$  vertex of element ' $k$ '. The list is ordered and counter-clockwise, hence, an edge  $E(EN(k,1), EN(k,2))$  is a directed edge which originates from the 1st vertex, terminates at the 2nd, and has the area of the element to its left. the search for an element  $k \in G_{old}$  which encloses a node  $S \in G_{new}$  is performed by the following procedure:

```

Procedure LOCATE(k,S)
  for i:=1,3 do
    j:=i+1 ; if j>3 then j:=1;
    if S lies to the right of E(NE(k,i), NE(k,j)) then
      find element k' which shares
      E(NE(k,i), NE(k,j)) with k;
      k:=k' ; LOCATE(k,S);

```

Upon entering the procedure LOCATE,  $\Omega$  is partitioned into a set of convex subregions and an arbitrary element ' $k$ ' is selected within the subregion which contains  $S$ . On exit ' $k$ ' is the desired element.

Various interpolation scheme can be used to approximate the value of  $\psi$ ,  $n$ , and  $p$  at  $S$ . A linear interpolant over each triangle is the simplest choice, but not necessarily the best. A more elaborate interpolation scheme based on the quadratic Bernstein polynomials is attractive. Although the computational cost of a non-linear interpolant is greater, but the trade off in terms of the overall solution time is favorable, since non-linear interpolants can provide a better initial guess for each solution stage. In particular, solving the device equations in a coupled mode, we have experience a reduction of about 10% in computation time, when switching from a linear to a quadratic Bernstein interpolant.

A function, 'f', whose nodal values on element 'k' is known can be expanded by the Bernstein polynomials:

$$(15) \quad f(L_1, L_2, L_3) = \sum_{|r|=3} \frac{3!}{i!j!m!} L_1^i L_2^j L_3^m \beta_{ijm} ,$$

where  $L_1, L_2, L_3$  are the normal area co-ordinates with respect to element 'k', the integers  $i, j, m$  can take values between 0 and 2,  $|r| = i+j+m$ , and the coefficients  $\beta_{ijm}$  can be computed using the nodal values of 'f' and its first derivatives, ' $\nabla f$ '. There are ten such coefficients (Frain 1986), nine of which are independent ( $\beta_{111}$  is expressed in terms of the other nine coefficients). To interpolate the value of 'f' to a point  $S$  in element 'k' one needs to consider a patch of elements as shown in Fig.(8),

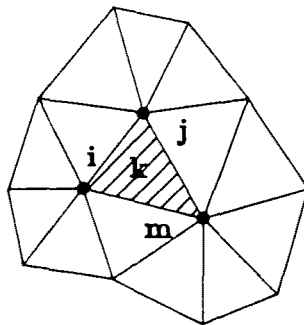


**Figure 8-** A Patch for the Computation of Bernstein Polynomials

where by exploiting the information stored in the NE list, ' $\nabla f$ ' is computed for all the elements sharing a vertex with 'k' and using an equation similar to (10) the nodal values of ' $\nabla f$ ' is computed. Since the nodal values of 'f' are also available, after appropriate co-ordinate transformation Eqn.(15) yields an

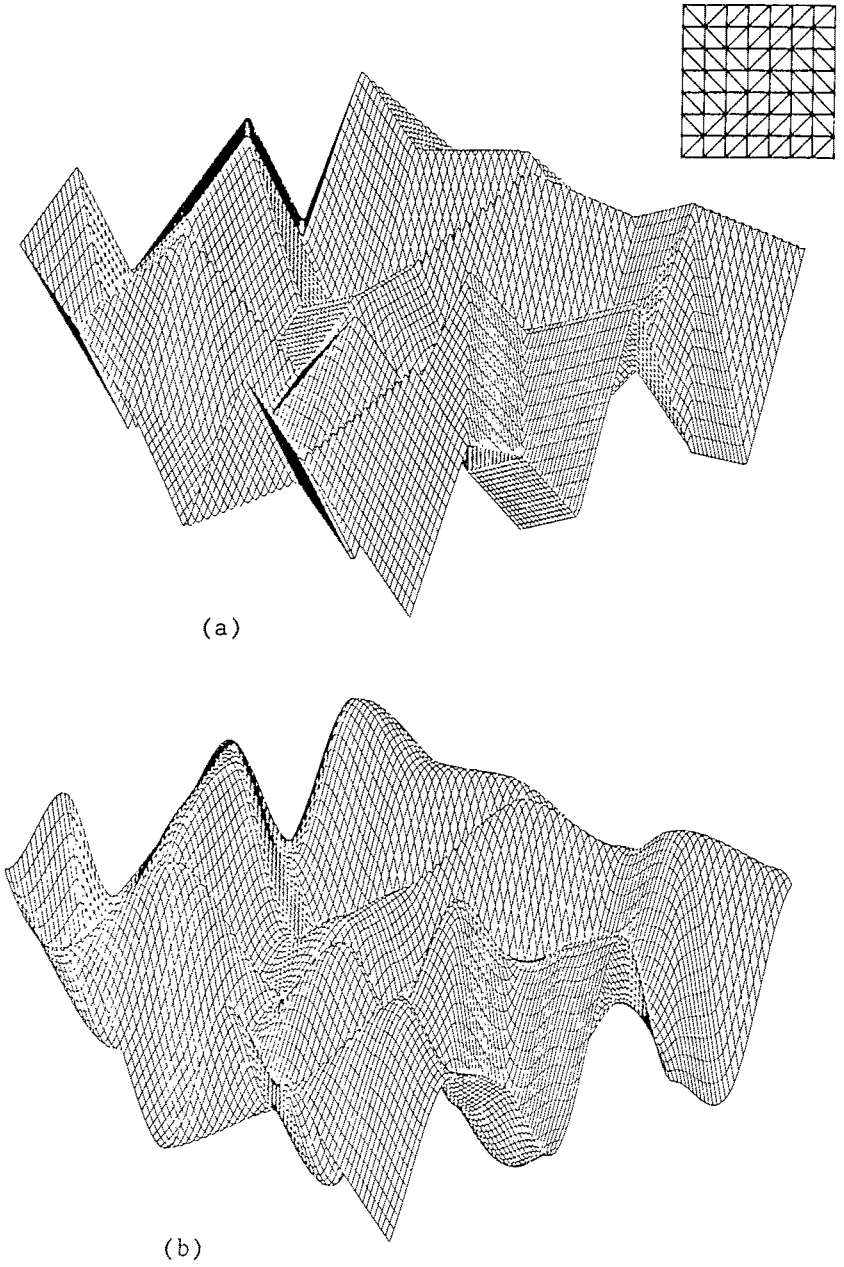


Figure 9- Interpolation for a randomly valued function:  
(a) Linear Interpolation,  
(b) Quadratic Bernstein Interpolation.

approximation to 'f' at the point S. We demonstrate the Bernstein interpolation by selecting a function randomly valued at the nodes of a triangular grid. The function after linear interpolation is plotted in Fig.(9a) and the smooth surface of Fig.(9b) is generated by the Bernstein interpolation scheme.  $\psi$ ,  $n$ , and  $p$  are also interpolated in the same fashion, where interpolating for the electrostatic potential the nodal values of  $\psi$ , and for electrons and holes the nodal values of  $\log(n)$  and  $\log(p)$  are used.

### 3. EXAMPLES

We demonstrate our adaptive scheme by means of three examples, namely, a p-n diode, a MESFET and a MOSFET. In accordance with the discretization of the device equations, the error indicator used here is based on the box method (Eqn.(12) and (13)).

#### 3.1 p-n Diode

In a p-n diode current densities dominantly flow perpendicular to the layer region at the p-n junction, and are smooth functions (Markowich 1986). The contribution from the continuity equation to the error indicator of Eqn.(14) is, therefore, small and Eqn.(12) is solely used to measure the error. We have conducted a numerical experiment on a p-n diode with elliptically rotated Gaussian profile, bulk density of  $N_A=10^{17} \text{ Cm}^{-3}$ , and a peak donor density of  $N_D=10^{18} \text{ Cm}^{-3}$ . Starting from a coarse mesh after 6 refinement cycle the grid of Fig.(10) is obtained. The refinement was performed close to the breakdown voltage, and it was noticed that the breakdown voltage is quite insensitive to the refinement in the depletion region (see Table 1).

TABLE 1- Grid Refinement Versus Breakdown Voltage

Refinement Stage	1	2	3	4	5	6
No. of Elements	136	180	238	296	403	549
Breakdown Voltage	18.63	18.41	18.07	18.06	18.02	18.02

This phenomenon can be explained by recalling that the current densities play an important role in the breakdown process, and since current density in a p-n diode is a smooth variable, it can be resolved by a mesh layout of moderate density and still yield accurate terminal characteristics.

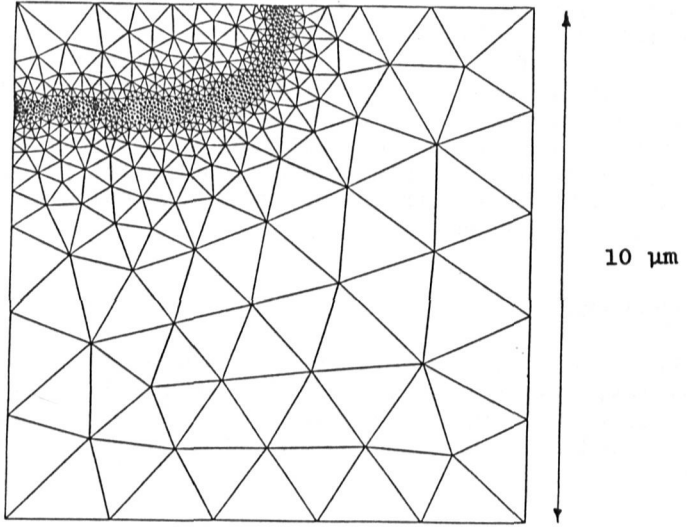


Figure 10- Grid Refinement for a p-n Diode.

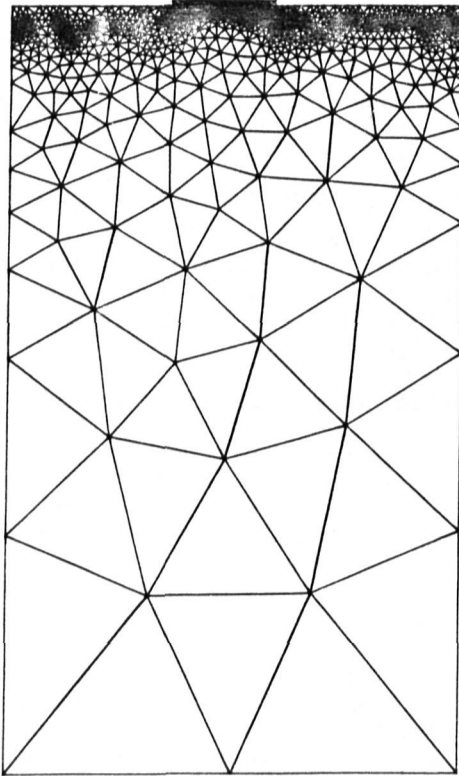


Figure 11a- MOSFET Grid after 7 refinement Cycles.

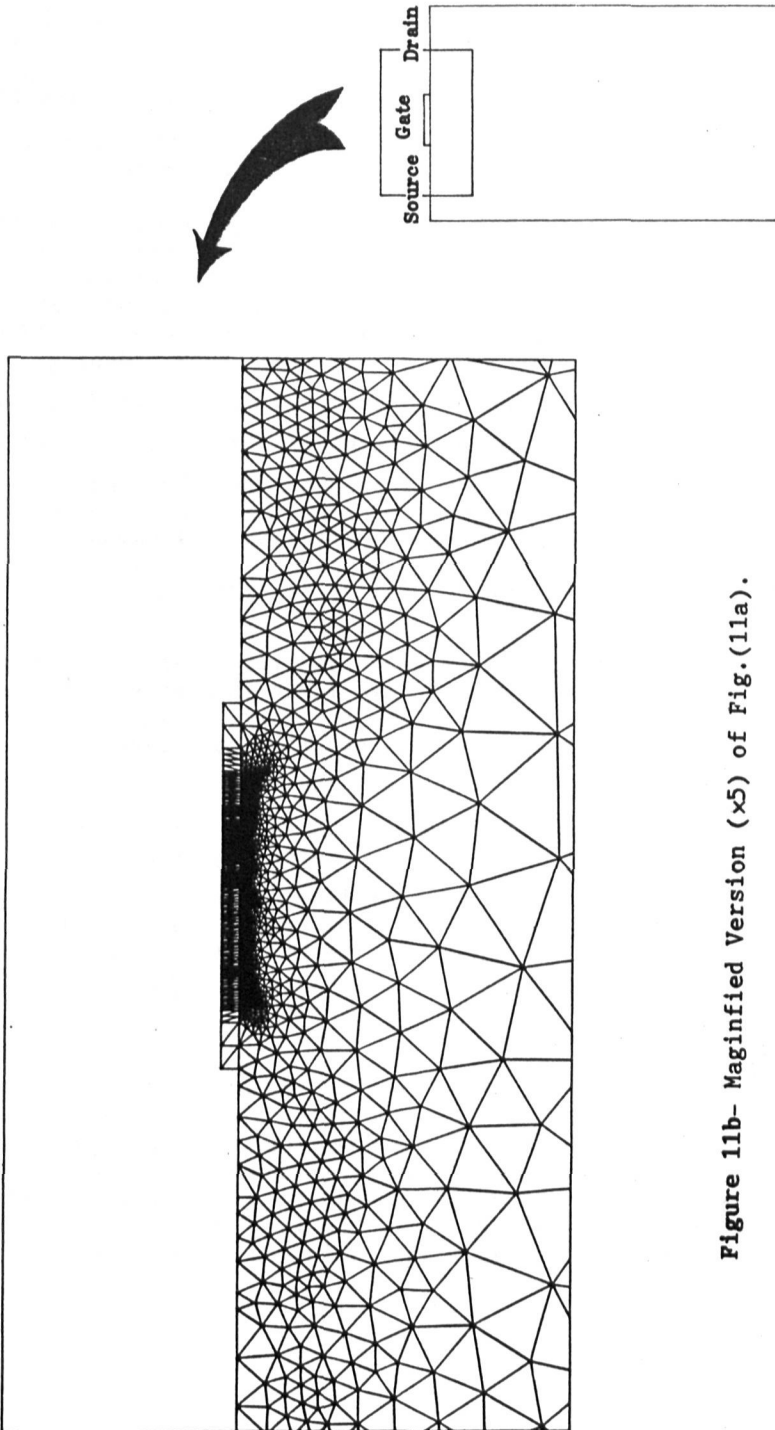


Figure 11b- Magnified Version (x5) of Fig.(11a).

### 3.2 MOSFET'S AND MESFET'S

In MOSFET's and MESFET's the current densities exhibit a layer behaviour, since they flow parallel to the layer region which is formed in the vicinity of the Shottcky contact for a MESFET or at the interfacial region of Si-SiO<sub>2</sub> in a MOSFET.

This behaviour is more pronounced in MOSFET's, where the width of the conducting channel can be a few tens of Angstrom.

An error indicator for such devices should, therefore, contain the error contribution from the continuity equation. Hence, Eqn.(14) is used to measure the error for each element. A numerical experiment was conducted on an n-channel MOSFET with a 1 μm metallurgical gate. The junction depth is 0.17μm, the oxide thickness is 500 Å and the bulk doping is  $N_A=10^{16} \text{Cm}^{-3}$ . The refinement was performed at  $V_{gs}=2.5$  Volts and  $V_{ds}=1$  Volts. After 7 refinement stages the grid of Fig.(11a) was obtained, where the number of elements is 3413. The grid is well refined in the channel and resolves the layer behaviour of the current densities. There is also some refinement in the depletion region of  $n^+-p$  (See Fig(11b)), which reflects the structure of the solution.

The MESFET chosen for the second experiment is a recessed gate GaAs MESFET having an active layer thickness of 0.4 μm, and the gate length of 0.75 μm. The Shottcky barrier height was chosen at 0.6 V, and a Gaussian profile was defined with the peak at  $N_D=2.5 \times 10^{17} \text{Cm}^{-3}$  located at the depth of 85nm. Six refinement cycles were performed in the saturation region ( $V_{ds}=4.5$  V) and at zero gate voltage. Starting from the initial grid of Fig.(12a), and after five refinement stages the refined grid of Fig.(12b) is achieved which possesses 2716 elements. It can be seen that the area in the vicinity of the Shottcky contact is well refined. The refinement is also denser on the drain side where the channel is pinched off and current densities rapidly vary.

Table 2 shows the effect of the refinement on the normalized drain current for these two devices. The currents are normalized with respect to the drain current computed at the last stage of the refinement. the drain current for the MOSFET is very sensitive to the refinement even in the later stages of the adaptive cycle. This is due to the fact that the current densities are confined to a very thin conducting channel and exhibit strong layer behaviour.



Figure 12b- MEFET Mesh after 5 refinement Cycles.



Figure 12a- Initial MEFET Mesh.

TABLE 2- Normalized Drain Current Versus Refinement

Refinement Stage	1	2	3	4	5	6	7
MOSFET $I_d/I_{d,7}$	1.09	0.96	0.71	0.89	0.93	0.96	1.00
MESFET $I_d/I_{d,7}$	0.92	0.95	1.02	0.99	1.00	—	—

Table 2 also suggests that, unlike MESFET's, accurate current calculation for MOSFET's require a very dense refinement and a large number of elements. This is especially true for the meshing strategies based on equi-angular triangulation.

### REFERENCES

ARMSTRONG, A., FERGUSON, R. S., and FLYN, J. G., 1986, Solution of semiconductor equations using a fully adaptive mesh strategy. *Elect. Lett.*, 22, 856-858.

BUTURLA, E. M., COTTREL, P. E., GROSSMAN, B. M., and SALSBERG, K. A., 1981, Finite-element analysis of semiconductor devices: The FIELDAY Program. *IBM J. Res. Develop.*, 25, 218-231.

DELJOUIE-RAKHSANDEH, K., DEELEY, E. M., 1988, Error indication and adaptive refinement in semiconductor device simulation. *Int. J. Electronics*, 64, (to appear)

DELJOUIE-RAKHSANDEH, K., 1988, An approach to generation and refinement of triangular grids possessing few obtuse triangles. Submitted to *Int. J. Num. Meth. Engng.*

FRAIN, G., 1986, Triangular Bernstein-Bezier patches. *Computer Aided Geometric Design* 3, 83-127.

FERNANDES, P., GIRDINO, P., MOLFINO, P., REPPETO, M., 1988, Local error estimates for adaptive mesh refinement. *IEEE Trans. Magnetics*, 24, 299-302.

GUERRIERI, R., and RUDAN, M., 1983, Optimization on the finite element solution of the semiconductor device Poisson equation. *IEEE Trans. Electron Devices*, ED-30, 1097-1103.

MARKOWICH, P. A., 1986, The stationary semiconductor device equations. (Wien: Springer-Verlag).

VAN WELIJ, J. S., 1986, Basis function matching tangential components on element edge. *SISDEP-86*, 371-383.

ZALMAL, M., 1986, Finite element solution of the fundamental equation of the semiconductor devices, *I. Math. Comp.*, **46**, 27-43.

ZIENKIEWICZ, O. C., and CRAIG, A., 1986, Adaptive refinement, error estimates, multigrid solution, and hierarchic finite element method concepts. In *Accuracy Estimates and Adaptive Refinement in Finite Element Computation*. I. Babuska et al. (Eds.), 25-29.

ZIENKIEWICZ, O. C., and ZHU, J. Z., 1987, A simple error estimator and adaptive procedure for practical engineering analysis. *Int. J. Num. Meth. Engng.*, **24**, 337-357.